Geophysical Research Letters

RESEARCH LETTER
10.1029/2021GL092436

# Caldera Collapse as the Trigger of Chaos and Fractured Craters on the Moon and Mars

**Erica Luzzi[1], Angelo Pio Rossi[1], Matteo Massironi[2], Riccardo Pozzobon[2], Giacomo Corti[3], and Daniele Maestrelli[3]**

[1]Department of Physics and Earth Sciences, Jacobs University Bremen, Bremen, Germany, [2]Dipartimento di Geoscienze, Università degli Studi di Padova, Padova, Italy, [3]CNR-IGG, The National Research Council of Italy, Institute of Geosciences and Earth Resources, Florence, Italy

**Key Points:**

- The formation mechanism that produced chaotic terrains and floor-fractured craters could be piecemeal caldera collapse
- The analog experimental models showed that $H_20$ did not necessarily have a primary role in the collapse of chaotic terrains
- The faults due to piecemeal caldera collapse are consistent with the faults' geometry in chaotic terrains and floor-fractured craters

**Supporting Information:**

Supporting Information may be found in the online version of this article.

**Correspondence to:**

E. Luzzi,
e.luzzi@jacobs-university.de

**Citation:**

Luzzi, E., Rossi, A. P., Massironi, M., Pozzobon, R., Corti, G., & Maestrelli, D. (2021). Caldera collapse as the trigger of Chaos and fractured craters on the Moon and Mars. *Geophysical Research Letters*, *48*, e2021GL092436. https://doi.org/10.1029/2021GL092436

Received 6 JAN 2021
Accepted 9 MAY 2021

**Author Contributions:**

**Conceptualization:** Erica Luzzi, Angelo Pio Rossi, Matteo Massironi, Riccardo Pozzobon
**Data curation:** Erica Luzzi, Giacomo Corti, Daniele Maestrelli
**Formal analysis:** Erica Luzzi, Daniele Maestrelli
**Funding acquisition:** Angelo Pio Rossi
**Investigation:** Erica Luzzi, Matteo Massironi, Riccardo Pozzobon, Giacomo Corti, Daniele Maestrelli
**Methodology:** Giacomo Corti, Daniele Maestrelli



**Abstract** Chaotic terrains are broad regions on Mars characterized by the disruption of the basaltic bedrock into polygonal blocks separated by deep fractures. To date, the proposed genetic scenarios often involve the occurrence of subsurface ice or liquid $H_2O$. Nevertheless, similar features also occur within some craters on the Moon, namely floor-fractured craters (FFCs), where water ice reservoirs are not present. We propose a new formation mechanism for Martian chaotic terrains as well as for lunar and Martian FFCs. The proposed mechanism does not require a major role of water but multiple cycles of inflation and deflation of a buried magma chamber. This process results in a particular type of caldera collapse, called the piecemeal (or chaotic) caldera collapse. A series of analog experiments show both geometrical and quantitative correspondence with natural case studies: Arsinoes Chaos (Mars), an unnamed FFC (Mars), and Komarov crater (FFC on the Moon).

**Plain Language Summary** The formation mechanism of peculiar chaotic terrains on Mars remains at the center of a long debate. To date, the most supported theories involve a primary role of water, either liquid or ice. Our experiments' goal was to demonstrate whether or not it was possible to reproduce the characteristic polygonal fractures of chaotic terrains through a volcano-tectonic process that does not require an interaction with water. We found very strong resemblances between our experiments' results and the morphology of chaotic terrains. The latter can also be compared to floor-fractured craters, which also occur on the Moon, and are believed to be formed by volcano-tectonic processes as well.

## 1. Introduction

### 1.1. Chaotic Terrains

Chaotic terrains are broad regions on Mars, often depressed and bordered by scarps, where the bedrock is characterized by large irregular mesas arranged chaotically (Sharp, 1973). Toward the inner part of the chaos, the mesas evolve into more and more eroded knobs. In some areas, hydrated minerals were found in the overlying light-toned layered deposits (Baioni & Tramontana, 2015; Glotch & Christensen, 2005; Lichtenberg et al., 2010; Massé et al., 2008; Sefton-Nash et al., 2012). Several formation mechanisms were proposed in literature to explain the collapse that generated the disruption of the bedrock in flat-topped blocks: they include groundwater overpressure within a confined aquifer (Andrews-Hanna & Phillips, 2007; Carr, 1979; Harrison & Grimm, 2009; Rodriguez et al., 2005; Warner et al., 2011), melting of a buried icy lake (Manker & Johnson, 1982; Roda et al., 2014; Zegers et al., 2010), interactions between magma and ice or water (Chapman & Tanaka, 2002; Head & Wilson, 2007; Leask et al., 2006; Meresse et al., 2008; Wilson & Head, 2002), intrusion of magmatic bodies and consequent inflation (Korteniemi et al., 2006), and instability of a large amount of underground clathrates (Hoffman, 2000; Kargel et al., 2007).

Nevertheless, when we invoke processes involving liquid water we have to consider that some chaotic terrains are not associated with outflow channels nor with any fluvial evidence (both erosional and depositional) and, equally importantly, that similar features also occur in the absence of water in floor-fractured craters (FFCs) on the Moon. In addition, there are no known analogs for such collapse-related features driven by subsurface ice or water action on Earth. Instead, around and within the chaotic terrains, a variety of volcano-tectonic features are predominant (Luzzi, Rossi, Carli, et al., 2020) such as pit chains (Mége et al., 2000; Tanaka, 1997) (Figure 1b), fissure vents associated with lava flows (Jaeger et al., 2010;

**Project Administration:** Angelo Pio Rossi
**Software:** Erica Luzzi
**Supervision:** Angelo Pio Rossi, Riccardo Pozzobon, Giacomo Corti
**Writing – original draft:** Erica Luzzi
**Writing – review & editing:** Angelo Pio Rossi, Matteo Massironi, Riccardo Pozzobon, Giacomo Corti, Daniele Maestrelli

Leone, 2014; Leverington, 2011), pitted cones (Meresse et al., 2008), and y-shaped conjunctions of fissures/grabens (Leone, 2014; Mège et al., 2003) (Figure 1b) possibly linked to inflation/deflation of shallow intrusions.

Pit chains have been considered as the result of dilational normal faulting (Ferrill et al., 2011; Wyrick et al., 2004), karst dissolution (Spencer & Fanale, 1990), extensional fractures (Tanaka & Golombek, 1989), collapsed buried conduits, particularly in the cases of sinuous patterns (Sauro et al., 2020), events of explosive activity due to magma-water interactions (Head & Wilson, 2007), and dyke intrusions (Cushing et al., 2015; Mège & Masson, 1996; Mége et al., 2000; Montési, 2001; Pozzobon et al., 2015; Scott & Wilson, 2002; Wilson & Head, 2002).

Pit chains are frequently coalescent and often associated with volcanic grabens (*sensu* Scott & Wilson, 2002). According to Mège et al. (2003), individual rift zones would form above elongated magma chambers: in the case of limited deflation, the surface expression of the dilatant deformation would result in pit chains; in the case of stronger deflation, the deformation would be enough to produce volcanic grabens.

### 1.2. Floor-Fractured Craters

The FFCs on the Moon strongly resemble chaotic terrains and share the same polygonal fractures; they are thought to be due to the emplacement of sub-volcanic magmatic intrusions through complex plumbing systems of dykes and sills (Head & Wilson, 2017; Jozwiak et al., 2012, 2015; Michaut et al., 2020). According to Wilson and Head (2018), after the emplacement of a laccolith, inflation would produce the stress responsible for fracturing and uplifting the overlying crater floor mainly at its edges. Accordingly, on the Moon, inflation caused by magmatic bodies has been already invoked for the formation of polygonal fractures. This hypothesis is also supported by gravity data: positive Bouguer anomalies were found in correspondence of FFCs, and interpreted as due to dense magma beneath the crater (Jozwiak et al., 2015, 2017; Thorey et al., 2015). Bamberg et al. (2014) described and mapped the global distribution of FFCs on Mars, recognizing two different groups: one related to fluvial activity and one where fluvial evidence is missing in contrast

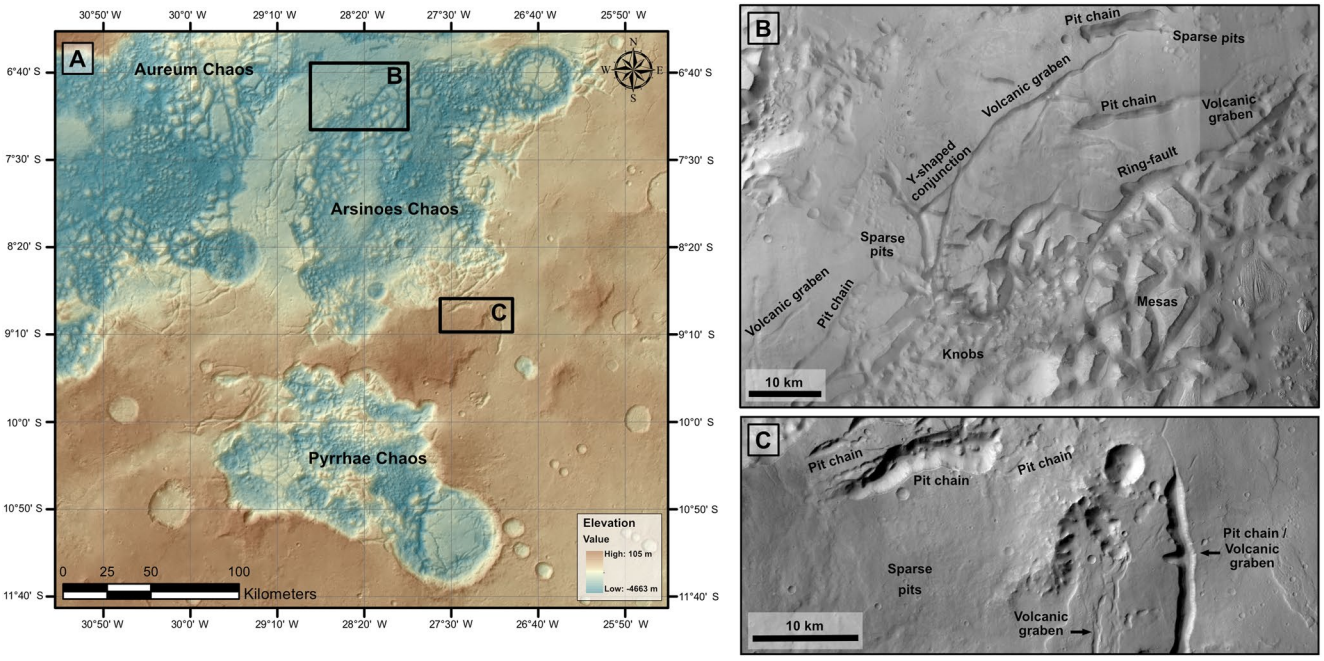


**Figure 1.** (a) Colored blend of the Digital Elevation Model (DEM) derived from the Mars Orbiter Laser Altimeter (MOLA) and the High-Resolution Stereo Camera (HRSC) (200 m/pixel) overlying with transparency a Context Camera (CTX) mosaic (6 m/pixel) for the location of Arsinoes Chaos, our analog case of study. (b)–(c) Examples of the recurrent volcano-tectonic features occurring in Arsinoes Chaos: volcanic grabens (*sensu* Scott & Wilson, 2002), pit chains, and sparse pits. The characteristic morphology of chaotic terrains is also shown (ring-fault, mesas, and knobs). CTX mosaic.

with a widespread occurrence of volcano-tectonic features. The second group has been interpreted by the authors as due to intrusive volcanism, similar to what has been proposed for the Moon.

For this work, we focused our attention on an unnamed FFC on Mars, south of Aram Chaos (0.1°S, 337.2°E), and the lunar FFC Komarov crater (24.5°N, 152.2°E). Komarov crater is a class 2 FFC, occurring in correspondence of Mare Moscoviense, where the predicted crust thickness has been proposed as spanning from 1 to 20 km (Wieczorek et al., 2013). Due to the thin crust, Morota et al. (2009) suggest that in this region, magma could have smoothly ascended from the mantle. Therefore, we consider Komarov crater as the best case scenario of magmatic activity in correspondence of FFCs. In fact, it exhibits distinctly the radial and concentric fractures characteristic of FFCs.

Walwer et al. (2021) conducted a study of correlation between floor uplift and the total fracture length within FFCs, assessing that the variability of this correlation seems to be due to the different overpressures in the intrusive bodies below the craters. In particular, the authors demonstrated that craters overlying a thinner crust suffer of a larger overpressure. Furthermore, they propose that the magma storage in the lunar crust could be ascribed to vertical dykes ascending from the crust-mantle interface. These results emphasize the fact that Komarov crater, with its thin crust below the crater and therefore large overpressure, might be one of the best sample lunar FFCs to test our hypothesis.

### 1.3. Piecemeal Caldera Collapse

The occurrence of widespread volcano-tectonic structures and the peculiar morphology of chaotic terrains and FFCs consisting of irregular polygonal blocks within depressed areas recall a process known as "piecemeal" or "chaotic" caldera collapse (Branney & Kokelaar, 1994; Moore & Kokelaar, 1998; Roche et al., 2000; Scandone, 1990; Troll et al., 2002; Walter & Troll, 2001), generated by multiple cycles of inflation and deflation of a buried magma chamber. Unlike the classic "piston collapse" where a coherent block collapses bounded by a ring fault which maintains the piston and the caldera floor undissected, in piecemeal caldera collapse, the subsidence causes the disruption of the piston, and the consequent dissection of the caldera floor into irregulars blocks (Lipman & Lipman, 1997; Roche et al., 2000). Branney and Kokelaar (1994) specify that the classification of piecemeal caldera includes both calderas with block-faulted floors and calderas where the polygonal blocks on the floor are missing because they have been turned into mega- and mesobreccia.

The existence of collapsed calderas on Mars in areas where volcanic edifices are not found was already proposed by Michalski and Bleacher (2013), who discussed the possibility that many depressions thought to be craters on Mars are instead the result of supervolcano collapses.

Furthermore, Leone (2014) and Leverington (2011) argued that magmatic processes are the simplest to explain many structural features occurring in Valles Marineris and within chaotic terrains such as pit chains, grabens, and lava-draped channels showing bifurcations.

In this work, we want to quantitatively constrain the processes leading to the formation of the polygonal blocks and the scarps that characterize chaotic terrains and FFCs.

We take Arsinoes Chaos (7.7°S, 332.1°E) as a case study for the development of chaotic terrains (Figure 1a). Arsinoes Chaos is a closed basin characterized by a sharp rim; therefore, in this area, it was easier to model a hypothetical analog magma chamber, as most of the other known chaotic terrains are more irregular and coalescent.

## 2. Materials and Methods

We tested the effect of repeated inflation-deflation cycles of a magma chamber on the resulting superficial pattern of deformation, by using a series of analog models with a setup similar to that illustrated in Walter and Troll (2001) and Troll et al. (2002). Specifically, our setup consisted of an elastic latex membrane fixed to a Plexiglas base able to expand when inflated with a magma analog. The membrane was pre-inflated to reach 1 cm in height during model building up so that a successive phase of deflation induced collapse. After pre-inflation, a layer of sand was poured on the membrane and flattened to obtain a uniform model

surface before deformation. This layer, intended to mimic the Martian and lunar overburden with a brittle behavior, was simulated by using K-feldspar sand. The sand (Colorobbia FS 900) has a density ($\rho$) of 706 kg $m^{-3}$, a cohesion (c) of ≈45 Pa and an angle of internal friction ($\phi$) of 62°, calculated according to the procedure described by Montanari et al. (2017). Its fine grain size (<40 μm) allowed a good detection of small fractures and faults developed on the model surface. An analog magma material was then inflated using a stepper motor piston, allowing for a constant injection velocity. Magma was simulated with Polyglicerine-3 (PG3) (Montanari et al., 2017).

We built up an experimental series composed of 10 models (for more information on the choice of the experiments see Text S1). Two similar setups were built: a "circular membrane" setup (here named setup S1) was designed to obtain a reference model, comparable with the setup of Walter and Troll (2001) and Troll et al. (2002). The latex membrane was designed with a diameter of 9 cm and pre-inflated to 1 cm in height (corresponding to 15 ml of pre-injected analog magma), on top of which a 0.5 cm thick overburden was layered. A second setup (setup S2) was designed to reproduce the plan view geometry of Arsinoes Chaos (i.e., having an irregular elliptical shape) with a major and a minor axis respectively of 9 and 5 cm and an overburden 0.6 cm thick. All other parameters were kept identical to setup S1.

A first cycle of inflation was started by injecting 20 ml of analog magma, then during the deflation, 20 ml of magma were withdrawn, and a second cycle was repeated by intruding 30 ml and withdrawing 40 ml. Tests with further cycles were also made but were proven to simply reactivate existing structures; therefore, we examined the models after two cycles.

In order to guarantee a correct comparison with the natural prototype, models were correctly scaled (Table S1) (King Hubbert, 1937; Ramberg, 1981; Weijermars & Schmeling, 1986). Geometrical scaling of lengths was set so that 1 cm in the model corresponds to 20 km in Arsinoes Chaos and 10 km in FFCs. This implies a model to nature length ratio $l^*$ (where $l^* = l_m/l_n$) equal to $5 \times 10^{-7}$ for Arsinoes and $l^* = 10^{-6}$ for the lunar FFC. The density scaling ratio $\rho^* = 0.271$ was calculated assuming a bulk crustal density of ≈2,600 kg $m^{-3}$ both for Mars and the Moon (e.g., Byrne et al., 2015; Wieczorek et al., 2013). The correct scaling of forces was obtained by considering the different gravities on Mars ($g \approx 3.71$ m/$s^2$) and on the Moon ($g \approx 1.62$ m/$s^2$), implying a gravity scaling ratio $g^*$ of 2.64 and 6.05, respectively. This allowed the calculation of the stress scaling ratio $\sigma^* = \rho^* g^* l^*$ which is $\approx 3.58 \times 10^{-7}$ for Mars and $1.64 \times 10^{-6}$ for the Moon. A correct dynamic scaling implies that the stress scaling ratio is equal to the ratio between material cohesion and natural rock cohesion ($\sigma^* = c^* = c_m/c_n$). From this, considering a material cohesion ($c_m$) of 45 Pa, we calculated a range of cohesion for natural rocks on Mars and Moon of $27.4 \times 10^6$–$12.5 \times 10^7$ Pa, which is consistent with natural values (e.g., Byrne et al., 2015). Finally, our models only reproduced and considered the brittle deformation (which is strain rate independent), and therefore, the kinematic scaling of velocities was not necessary.

The stereophotogrammetry to produce Digital Elevation Models (DEMs) of the experiment was performed using Agisoft Metashape, where point cloud-based DEMs were computed.

The imagery used in this work consists of Context Camera (CTX) images (resolution of 6 m/pixel) collected by the Mars Reconnaissance Orbiter (Malin et al., 2007), which were processed into a global mosaic and made public by the Murray lab (Dicksonet al., 2018). The DEM used for the measurements is a blend between the Mars Orbiter Laser Altimeter (MOLA) (Smith et al., 1999) data and the High-Resolution Stereo Camera (HRSC) (Neukum & Jaumann, 2004) data, with a resolution of 200 meters/pixel.

The image of the Moon is cropped from the Lunar Reconnaissance Orbiter Camera (LROC) (Robinson et al., 2010) Wide Angle Camera (WAC) Global Morphology Mosaic (resolution of 100 m/pixel) provided by the USGS. The DEM used for the measurements of the lunar FFC is a merged product of the Lunar Orbiter Laser Altimeter (Smith et al., 2010) and the SELenological and Engineering Explorer (SELENE) (Ohtake et al., 2008) Kaguya data sets (resolution of 59 m/pixel).

## 3. Experiments and Implications

In order to test the piecemeal caldera collapse as a formation mechanism for chaotic terrains and FFCs, we set up a series of analog experiments to be compared to Arsinoes Chaos, the unnamed FFC on Mars and Komarov crater on the Moon. We present the results of two experiments, exemplificative of the behavior of

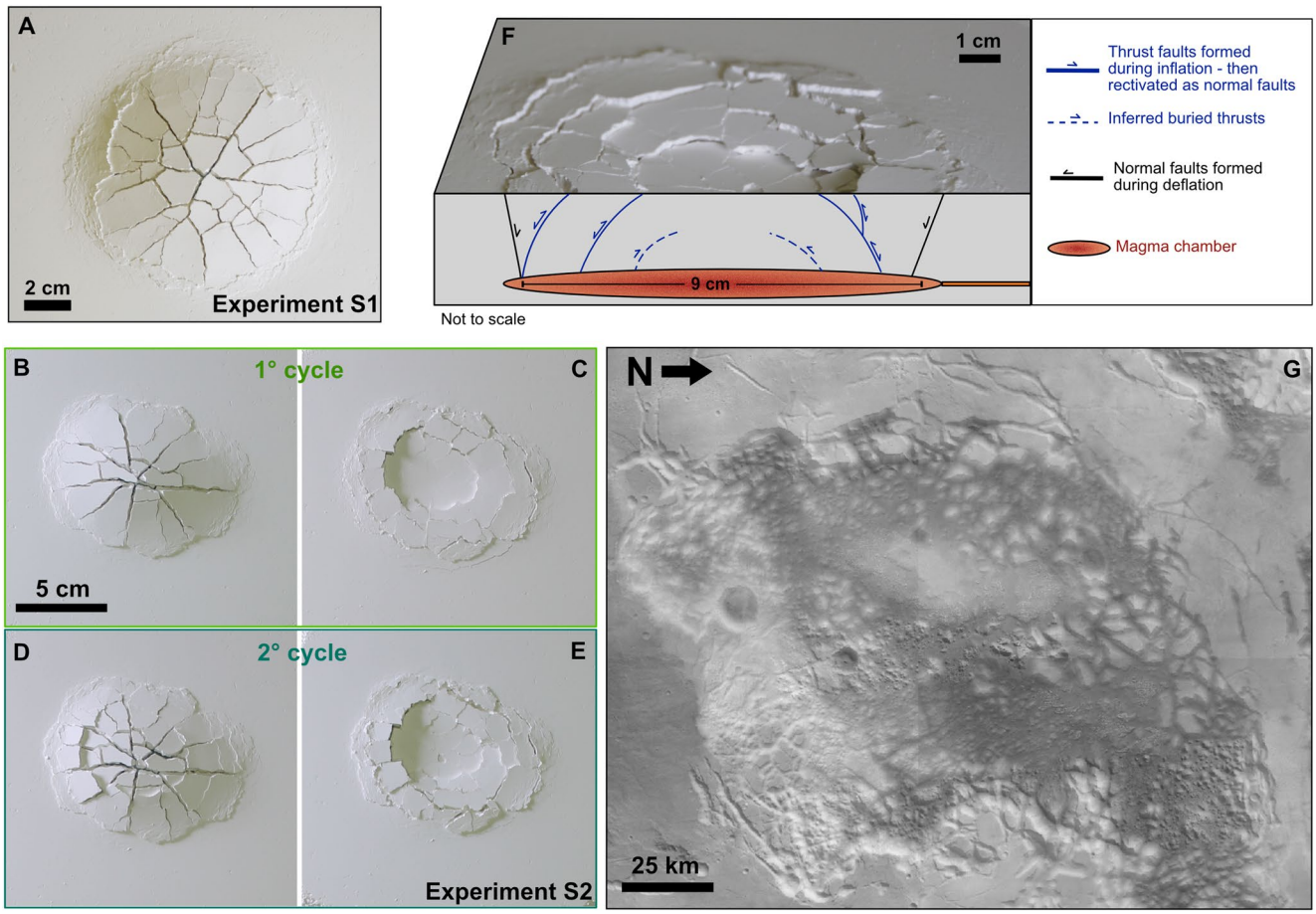


**Figure 2.** The results of the experiments are shown and compared to the morphology in Arsinoes Chaos. (a) Setup S1 at the end of the first intrusion. (b) Setup S2, elliptic magma chamber, first cycle, first inflation. Concentric thrusts are formed almost directly overlying the perimeter of the magma chamber, radial faults radiate from the top of the inflated mound. (c) First cycle, first deflation, setup S2. The concentric thrusts are re-activated as normal faults, new concentric faults are also formed. The caldera shows an irregular elliptical shape. The intersection between radial and concentric faults creates the polygonal blocks. (d) Second cycle, second inflation, setup S2. New concentric and radial faults are formed. (e) Second cycle, second deflation, setup S2. The floor collapsed further than at the end of the first cycle. (f) Interpretative cross-section of (e). Note that the thrusts formed during the first intrusion are then reactivated as normal faults during the magma withdrawal. Not to scale. (g) Digital Elevation Model superimposed in semi-transparency over the Context Camera mosaic, showing the morphology of Arsinoes Chaos, as disrupted polygonal blocks.

setup S1 (magma chamber with circular geometry reflecting the FFC natural cases on Mars and the Moon; Figure 2a) and setup S2 (magma chamber with irregular elliptical shape reproducing the geometry of Arsinoes Chaos' rim; Figure 2g).

In both the experiments, during the first inflation the bulging starts developing and the first structures formed are radial dilational faults and concentric thrusts bordering the periphery of the buried magma chamber (Figure 2b). During the first deflation (Figure 2c), at the end of the withdrawing, the bulge is collapsed, the thrusts are reactivated as normal faults and the outermost concentric normal faults are identified as the ring fault system as defined by Acocella (2007), while other concentric faults combined with the previously formed radial faults produce the peculiar polygonal geometries bounding the angular blocks. At the second inflation (Figure 2d) more radial dilational faults are produced and the bulge presents a collapsed top. The cycles end with the second deflation (Figure 2e), during which the ring fault undergoes a major subsidence, new radial and concentric structures form, and the pre-existing are enhanced.

The structures formed during the piecemeal collapse fit with the geometries identified on chaotic terrains and FFCs. The qualitative comparisons are shown in Figure 3. The circular setup S1 generated a circular caldera consistent with the FFCs, with radial and concentric faults, polygonal blocks and a caldera floor

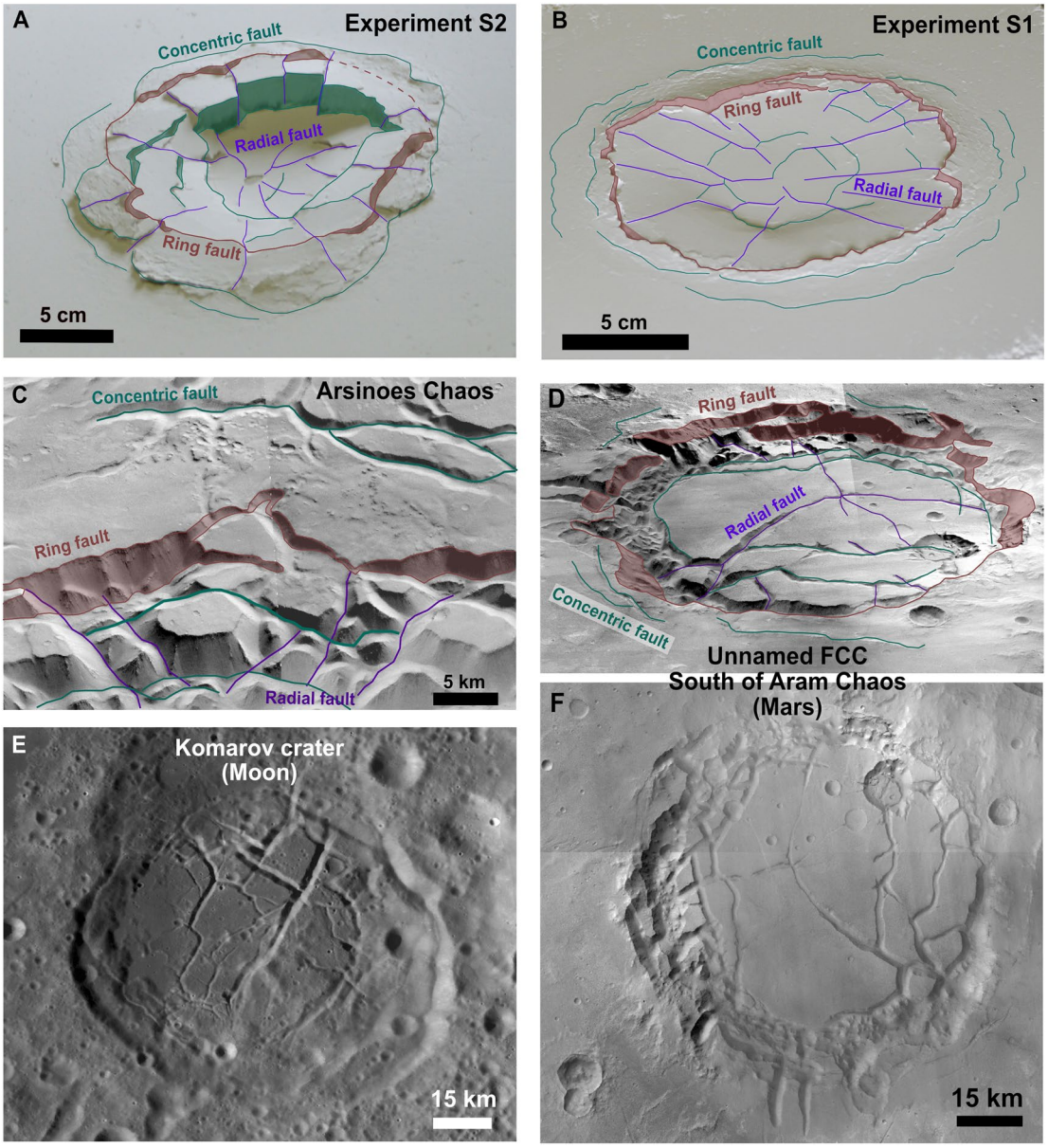


**Figure 3.** Comparison of the structures formed within the setup S2 experiment (a) and the structures occurring in Arsinoes Chaos (c) (Context Camera [CTX] mosaic and blended Mars Orbiter Laser Altimeter and the High-Resolution Stereo Camera [MOLA-HRSC] Digital Elevation Model [DEM]). The complexity in the natural case on Mars is augmented by millions years of erosion and by the occurrence of sedimentary infillings in the central part of the chaos, but both radial and concentric faults (purple and green) are still visible as well as the pronounced ring fault (brick red). Setup S1 (b) can be correlated with the unnamed floor-fractured crater (FFC) south of Aram Chaos (d) and (f) (CTX mosaic). (e) On the Moon, the FFC shares structures comparable to the setup S1 (Lunar Reconnaissance Orbiter Camera Wide Angle Camera Global Morphology Mosaic, 100 m/pixel).

bordered by the ring fault. The setup S2 formed an elongated caldera consistent with the more irregular basin of Arsinoes Chaos and in this case the structures formed during the experiment also fit very well with the natural case.

The measurements performed on the structures of the experiments and the comparison with the natural cases are reported in Table 1. The results indicate that the extent of the ring fault is consistent for all the experiments and natural cases, and so are the angles between the fractures that border the polygonal blocks and the subsidence along the ring fault. In particular, the consistency of the angles (Text S2 and Figure S1)

**Table 1**
*Comparison Between the Experiment's Geometries and the Natural Cases (Arsinoes Chaos, Mars; Unnamed FFC, Mars; Komarov Crater, Moon)*

| Scaled parameters (1:10) | Experiment S1 (after first cycle) | Experiment S1 (after second cycle) | Unnamed FFC (Mars) | Komarov crater (Moon) |
|---|---|---|---|---|
| Magma chamber perimeter | 28.6 cm (286 km) | 28.6 cm (286 km) | ? | ? |
| Magma chamber depth | 0.5 cm (5 km) | 0.5 cm (5 km) | ? | ? |
| Radial faults (max length) | 4.2 cm (42 km) | 4.6 cm (46 km) | 40 km | 51 km |
| Radial faults (average length) | 3 cm (30 km) | 3 cm (30 km) | 20 km | 30 km |
| Ring fault perimeter | 30 cm (300 km) | 30 cm (300 km) | 240 km | 280 km |
| Ring fault subsidence | 0.35 cm (3.5 km) | 0.45 cm (4.5 km) | 1–2 km | 1–3 km |
| Concentric periphery faults (max length) | 8.2 cm (82 km) | 8.2 cm (82 km) | 34 km | 53 km |
| Concentric periphery faults (average length) | 3 cm (30 km) | 7.6 cm (76 km) | 32 km | 45.5 km |
| Average angle between fractures | - | 95° | 95° | 95° |

| Scaled parameters (1:20) | Experiment S2 (after first cycle) | Experiment S2 (after second cycle) | Arsinoes Chaos (Mars) |
|---|---|---|---|
| Magma chamber perimeter | 46 cm (920 km) | 46 cm (920 km) | ? |
| Magma chamber depth | 0.6 cm (12 km) | 0.6 cm (12 km) | ? |
| Radial faults (max length) | 3.2 cm (64 km) | 4.6 cm (92 km) | 40 km |
| Radial faults (average length) | 2.5 cm (50 km) | 3.6 cm (72 km) | 27 km |
| Ring fault perimeter | 27 cm (540 km) | 27 cm (540 km) | 593 km |
| Ring fault subsidence | 0.05 cm (1 km) | 0.15 cm (3 km) | 1–4 km |
| Concentric periphery faults (max length) | 6.3 cm (160 km) | 6.3 cm (160 km) | 87 km |
| Concentric periphery faults (average length) | 4 cm (80 km) | 4.7 cm (94 km) | 60.5 km |
| Average angle between fractures | - | 97° | 95° |

Abbreviation: FFC, floor-fractured crater.

between the fractures assumes a crucial importance since it is not affected by unknown variables (especially by gravity) but purely reflects the process that generated a given stress field.

The main difference between the measures on the experiments and those on the natural cases consists of the length of radial and concentric faults, the scaled faults length in the experiment being generally larger than the natural case. Nevertheless, in the natural cases the geological setting has been modified, eroded, and covered by new deposits, over millions or billions of years; hence, it is reasonable to assume that at the time of their formation the faults could have had a larger extent and could have been hidden afterward, overprinted by subsequent events. On the other hand, the scarp of the ring fault might have suffered scarp retreat processes, hence the ring fault might have been slightly smaller at the formation time with respect to the current extent.

In general, the results of our experiment fit very well with the morphology characterizing FFCs and chaotic terrains. The generation of polygonal angular blocks within a depressed caldera and the abundance of concentric and radial faults are indeed consistent (Figures 3a and 3b), as well as the occurrence of a caldera floor where other deposits could be unconformably deposited in a subsequent sedimentary environment. Our interpretation may extend to other chaotic terrains and other floor-fractured craters on the Moon and Mars. Further work will be focused on investigating the effect of different crustal thicknesses beneath the collapses and depth of the magma source. Especially for lunar FFCs, several constraints need to be considered for the broader applicability of these results, since Komarov crater represents a best case scenario due to its previously described characteristics.

We were not able to test the unconfined setting because reproducing an unconfined experimental setup is a particularly complex task. In fact, the analog experiments are confined by their nature. Nonetheless, we

provide two possible explanations for the irregularity and coalescence of unconfined chaotic terrains: (a) the coalescence might have been caused by subsequent events that overprinted the pre-existing structures related to the caldera collapse, while at the time of the collapse all the chaotic terrains were confined; (b) the coalescence might have been caused by the proximity of multiple magma chambers. In fact, the occurrence of widespread pit chains, volcanic grabens, pitted cones, and basaltic mineralogies suggest the past presence of a magmatic province in the area; therefore, it could be plausible that multiple magma chambers were distributed in the region.

As for the FFCs, based on these preliminary results we cannot exclude that only one cycle of inflation and subsequent deflation (related to cooling processes) occurred, as agreed by the majority of the scientific community. We propose two cycles of inflation and deflation because (a) the results of our experiments show consistency; (b) it is more likely that during a 200 Ma volcanic activity (estimated by Morota et al., 2009) multiple events occurred, especially in craters overlying a thin crust as in Komarov crater, where Walwer et al. (2021) predicted a large overpressure of the magmatic body underneath the crater. Future work will be focused on assessing whether this formation mechanism can be held responsible with a major degree of certainty for the fracturing of FFCs or not.

## 4. Conclusions

Our analog experiment demonstrated that piecemeal caldera collapses can generate all the structural features occurring within confined chaotic terrains: a bordering normal ring fault, as well as the radial and concentric faults intersecting each other bordering polygonal angular blocks. We, thus, demonstrated that the occurrence of liquid water or ice is not essential to cause collapse and chaotic terrains. This would also explain the lack of outflow channel or any fluvial evidence in some chaotic terrains such as Arsinoes Chaos, as well as the resemblance between chaotic terrains and floor-fractured craters on the Moon, where water is not present and where laccolith-induced inflation was already proposed as a formation mechanism.

We do not exclude that on Mars, water (either liquid or ice) could have been present at the time of the caldera formation and might have augmented the intensity of the collapse and induced phreatomagmatic explosions (e.g., Korteniemi et al., 2006), but it seems not to have been the main driver.

Our results bring new insight into the formation mechanisms that generated chaotic terrains and FFCs, which are not always so chaotic as they might appear at a first glance, and call into question the involvement of water in the collapse history leading to their formation on Mars.

## Data Availability Statement

The data used in this work are stored in a repository following the FAIR principles (Luzzi, Rossi, Massironi, et al., 2020).

**Acknowledgments**
The authors acknowledge support and funding from the European Union's Horizon 2020 research and innovation program under grant agreement Nº776276 (PLANMAP). The authors want to express our appreciation to Dr. Jack Wright for improving the language quality of the manuscript, and to the reviewers for their constructive comments.

## References

Acocella, V. (2007). Understanding caldera structure and development: An overview of analogue models compared to natural calderas. *Earth-Science Reviews*, *85*(3–4), 125–160. https://doi.org/10.1016/j.earscirev.2007.08.004

Andrews-Hanna, J. C., & Phillips, R. J. (2007). Hydrological modeling of outflow channels and chaos regions on Mars. *Journal of Geophysical Research*, *112*(E8). https://doi.org/10.1029/2006je002881

Baioni, D., & Tramontana, M. (2015). Evaporite karst in three interior layered deposits in Iani Chaos, Mars. *Geomorphology*, *245*, 15–22. https://doi.org/10.1016/j.geomorph.2015.05.018

Bamberg, M., Jaumann, R., Asche, H., Kneissl, T., & Michael, G. G. (2014). Floor-fractured craters on mars - Observations and origin. *Planetary and Space Science*, *98*, 146–162. https://doi.org/10.1016/j.pss.2013.09.017

Branney, M. J., & Kokelaar, P. (1994). Volcanotectonic faulting, soft-state deformation, and rheomorphism of tuffs during development of a piecemeal caldera, English Lake District. *The Geological Society of America Bulletin*, *106*(4), 507–530. https://doi.org/10.1130/0016-7606(1994)106<0507:vfssda>2.3.co;2

Byrne, P. K., Holohan, E. P., Kervyn, M., De Vries, B. V. W., & Troll, V. R. (2015). Analogue modelling of volcano flank terrace formation on Mars. *Geological Society, London, Special Publications*, *401*(1), 185–202. https://doi.org/10.1144/SP401.14

Carr, M. H. (1979). Formation of Martian flood features by release of water from confined aquifers. *Journal of Geophysical Research*, *84*(B6), 2995. https://doi.org/10.1029/JB084iB06p02995

Chapman, M., & Tanaka, K. L. (2002). Related Magma-Ice Interactions: Possible Origins of Chasmata, Chaos, and Surface Materials in Xanthe, Margaritifer, and Meridiani Terrae, Mars. *Icarus*, *155*(2), 324–339. https://doi.org/10.1006/icar.2001.6735

Cushing, G. E., Okubo, C. H., & Titus, T. N. (2015). Atypical pit craters on Mars: New insights from THEMIS, CTX, and HiRISE observations. *Journal of Geophysical Research: Planets*, *120*(6), 1023–1043. https://doi.org/10.1002/2014JE004735

Dickson, J., Kerber, L., Fassett, C., & Ehlmann, B. (2018). A global, blended CTX mosaic of Mars with vectorized seam mapping: A new mosaicking pipeline using principles of non-destructive image editing. *Lunar and Planetary Science Conference*.

Ferrill, D. A., Wyrick, D. Y., & Smart, K. J. (2011). Coseismic, dilational-fault and extension-fracture related pit chain formation in Iceland: Analog for pit chains on Mars. *Lithosphere*, *3*(2), 133–142. https://doi.org/10.1130/L123.1

Glotch, T. D., & Christensen, P. R. (2005). Geologic and mineralogic mapping of Aram Chaos: Evidence for a water-rich history. *Journal of Geophysical Research*, *110*, 1–21. https://doi.org/10.1029/2004JE002389

Harrison, K. P., & Grimm, R. E. (2009). Regionally compartmented groundwater flow on Mars. *Journal of Geophysical Research*, *114*(E4). https://doi.org/10.1029/2008je003300

Head, J. W., & Wilson, L. (2007). Heat transfer in volcano-ice interactions on Mars: Synthesis of environments and implications for processes and landforms. *Annals of Glaciology*, *45*, 1–13. https://doi.org/10.3189/172756407782282570

Head, J. W., & Wilson, L. (2017). Generation, ascent and eruption of magma on the Moon: New insights into source depths, magma supply, intrusions and effusive/explosive eruptions (Part 2: Predicted emplacement processes and observations). *Icarus*, *283*, 176–223. https://doi.org/10.1016/j.icarus.2016.05.031

Hoffman, N. (2000). White Mars: A new model for mars' surface and atmosphere based on CO2. *Icarus*, *146*(2), 326–342. https://doi.org/10.1006/ICAR.2000.6398

Jaeger, W. L., Keszthelyi, L. P., Skinner, J. A., Milazzo, M. P., McEwen, A. S., Titus, T. N., et al. (2010). Emplacement of the youngest flood lava on Mars: A short, turbulent story. *Icarus*, *205*(1), 230–243. https://doi.org/10.1016/j.icarus.2009.09.011

Jozwiak, L. M., Head, J. W., III, Neumann, G. A., & Wilson, L. (2017). Observational constraints on the identification of shallow lunar magmatism: Insights from floor-fractured craters. *Icarus*, *283*, 224–231. https://doi.org/10.1016/j.icarus.2016.04.020

Jozwiak, L. M., Head, J. W., & Wilson, L. (2015). Lunar floor-fractured craters as magmatic intrusions: Geometry, modes of emplacement, associated tectonic and volcanic features, and implications for gravity anomalies. *Icarus*, *248*, 424–447. https://doi.org/10.1016/j.icarus.2014.10.052

Jozwiak, L. M., Head, J. W., Zuber, M. T., Smith, D. E., & Neumann, G. A. (2012). Lunar floor-fractured craters: Classification, distribution, origin and implications for magmatism and shallow crustal structure. *Journal of Geophysical Research*, *117*(11). https://doi.org/10.1029/2012JE004134

Kargel, J. S., Furfaro, R., Prieto-Ballesteros, O., Rodriguez, J. A. P., Montgomery, D. R., Gillespie, A. R., et al. (2007). Martian hydrogeology sustained by thermally insulating gas and salt hydrates. *Geology Series*, *35*(11), 975–978. https://doi.org/10.1130/g23783a.1

King Hubbert, M. (1937). Theory of scale models as applied to the study of geologic structures. *The Geological Society of America Bulletin*, *48*(10), 1459–1520. https://doi.org/10.1130/GSAB-48-1459

Korteniemi, J., Aittola, M., Öhman, T., Raitala, J., Korteniemi, J., & Öhman, T. (2006). *Floor-fractured craters on the terrestrial planets-The martian perspective Craterlake Geotrail Project View project floor-fractured craters on the terrestrial planets-the martian perspective*. Retrieved from https://www.researchgate.net/publication/228889992

Leask, H. J., Wilson, L., & Mitchell, K. L. (2006). Formation of Aromatum Chaos, Mars: Morphological development as a result of volcano-ice interactions. *Journal of Geophysical Research*, *111*(E8). https://doi.org/10.1029/2005je002549

Leone, G. (2014). A network of lava tubes as the origin of Labyrinthus Noctis and Valles Marineris on Mars. *Journal of Volcanology and Geothermal Research*, *277*, 1–8. https://doi.org/10.1016/j.jvolgeores.2014.01.011

Leverington, D. W. (2011). A volcanic origin for the outflow channels of Mars: Key evidence and major implications. *Geomorphology*, *132*, 51–75. https://doi.org/10.1016/j.geomorph.2011.05.022

Lichtenberg, K. A., Arvidson, R. E., Morris, R. V., Murchie, S. L., Bishop, J. L., Fernandez Remolar, D., et al. (2010). Stratigraphy of hydrated sulfates in the sedimentary deposits of Aram Chaos, Mars. *Journal of Geophysical Research*, *115*(E6). E00D17. https://doi.org/10.1029/2009JE003353

Lipman, P. W., & Lipman, P. W. (1997). Subsidence of Ash-Flow Calderas: Relation to Caldera Size and Magma-Chamber Geometry (Vol. 59). Springer-Verlag.

Luzzi, E., Rossi, A. P., Carli, C., & Altieri, F. (2020). Tectono-magmatic, sedimentary, and hydrothermal history of arsinoes and pyrrhae chaos, Mars. *Journal of Geophysical Research: Planets*, *125*. https://doi.org/10.1029/2019JE006341

Luzzi, E., Rossi, A. P., Massironi, M., Pozzobon, R., Maestrelli, D., & Corti, G. (2020). *Dataset: Caldera collapse as the trigger of chaos and fractured craters on the Moon and Mars*. Retrieved from https://data.4tu.nl/articles/dataset/Dataset_Caldera_collapse_as_the_trigger_of_Chaos_and_fractured_craters_on_the_Moon_and_Mars/13280417

Malin, M. C., Bell, J. F., Cantor, B. A., Caplinger, M. A., Calvin, W. M., Clancy, R. T., & Wolff, M. J. (2007). Context camera investigation on board the mars reconnaissance orbiter. *Journal of Geophysical Research*, *112*(E5). https://doi.org/10.1029/2006je002808

Manker, J. P., & Johnson, A. P. (1982). Simulation of Martian chaotic terrain and outflow channels. *Icarus*, *51*(1), 121–132. https://doi.org/10.1016/0019-1035(82)90032-X

Massé, M., Le Mouélic, S., Bourgeois, O., Combe, J.-P., Le Deit, L., Sotin, C., et al. (2008). Mineralogical composition, structure, morphology, and geological history of Aram Chaos crater fill on Mars derived from OMEGA Mars Express data. *Journal of Geophysical Research*, *113*. 12006. https://doi.org/10.1029/2008JE003131

Mège, D., Cook, A. C., Garel, E., Lagabrielle, Y., & Cormier, M. H. (2003). Volcanic rifting at Martian grabens. *Journal of Geophysical Research*, *108*(5), 10–11. https://doi.org/10.1029/2002je001852

Mége, D., Lagabrielle, Y., Garel, E., Cormier, M., & Cook, A. (2000). *Collapse features and narrow grabens on Mars and Venus: Dike emplacement and deflation of underlying magma chamber*.

Mège, D., & Masson, P. (1996). Amounts of crustal stretching in Valles Marineris, Mars. *Planetary and Space Science*, *44*(8), 749–781. https://doi.org/10.1016/0032-0633(96)00013-x

Meresse, S., Costard, F., Mangold, N., Masson, P., Neukum, G., & others (2008). Formation and evolution of the chaotic terrains by subsidence and magmatism: Hydraotes Chaos, Mars. *Icarus*, *194*(2), 487–500. https://doi.org/10.1016/j.icarus.2007.10.023

Michalski, J. R., & Bleacher, J. E. (2013). Supervolcanoes within an ancient volcanic province in Arabia Terra, Mars. *Nature*, *502*(7469), 47–52. https://doi.org/10.1038/nature12482

Michaut, C., Pinel, V., & Maccaferri, F. (2020). Magma ascent at floor-fractured craters diagnoses the lithospheric stress state on the Moon. *Earth and Planetary Science Letters*, *530*, 115889. https://doi.org/10.1016/j.epsl.2019.115889

Montanari, D., Bonini, M., Corti, G., Agostini, A., & Del Ventisette, C. (2017). Forced folding above shallow magma intrusions: Insights on supercritical fluid flow from analogue modeling. *Journal of Volcanology and Geothermal Research*, *345*, 67–80. https://doi.org/10.1016/j.jvolgeores.2017.07.022

Montési, L. G. J. (2001). Concentric dikes on the flanks of Pavonis Mons: Implications for the evolution of martian shield volcanoes and mantle plumes. *Special Papers - Geological Society of America*, *352*, 165–181. https://doi.org/10.1130/0-8137-2352-3.165

Moore, I., & Kokelaar, P. (1998). Tectonically controlled piecemeal caldera collapse: A case study of Glencoe volcano, Scotland. *Geological Society of America Bulletin*, *110*(11). https://doi.org/10.1130/0016-7606(1998)110<1448:tcpcca>2.3.co;2

Morota, T., Haruyama, J., Honda, C., Ohtake, M., Yokota, Y., Kimura, J., et al. (2009). Mare volcanism in the lunar farside Moscoviense region: Implication for lateral variation in magma production of the Moon. *Geophysical Research Letters*, *36*(21). L21202. https://doi.org/10.1029/2009GL040472

Neukum, G., & Jaumann, R. (2004). *HRSC: The High resolution Stereo Camera of Mars express*.

Ohtake, M., Haruyama, J., Haruyama, J., Matsunaga, T., Yokota, Y., Morota, T., & Honda, C. (2008). Performance and scientific objectives of the SELENE (KAGUYA) multiband imager. *Earth Planets and Space*, *60*(4), 257–264. https://doi.org/10.1186/BF03352789

Pozzobon, R., Mazzarini, F., Massironi, M., & Marinangeli, L. (2015). Self-similar clustering distribution of structural features on Ascraeus Mons (Mars): Implications for magma chamber depth. *Geological Society, London, Special Publications*, *401*(1), 203–218. https://doi.org/10.1144/sp401.12

Ramberg, H. (1981). *Gravity, deformation and the earth's crust : In theory, experiments, and geological application*.

Robinson, M. S., Brylow, S. M., Tschimmel, M., Humm, D., Lawrence, S. J., Thomas, P. C., et al. (2010). Lunar reconnaissance orbiter camera (LROC) instrument overview. *Space Science Reviews*, *150*(1–4), 81–124. https://doi.org/10.1007/s11214-010-9634-210.1007/978-1-4419-6391-8_6

Roche, O., Druitt, T. H., & Merle, O. (2000). Experimental study of caldera formation. *Journal of Geophysical Research*, *105*(B1), 395–416. https://doi.org/10.1029/1999jb900298

Roda, M., Kleinhans, M. G., Zegers, T. E., & Oosthoek, J. H. P. (2014). Catastrophic ice lake collapse in Aram Chaos, Mars. *Icarus*, *236*, 104–121. https://doi.org/10.1016/j.icarus.2014.03.023

Rodriguez, J., Sasaki, S., Kuzmin, R., Dohm, J., Tanaka, K., Miyamoto, H., et al. (2005). Outflow channel sources, reactivation, and chaos formation, Xanthe Terra, Mars. *Icarus*, *175*(1), 36–57. https://doi.org/10.1016/j.icarus.2004.10.025

Sauro, F., Pozzobon, R., Massironi, M., De Berardinis, P., Santagata, T., & De Waele, J. (2020). Lava tubes on Earth, Moon and Mars: A review on their size and morphology revealed by comparative planetology. *Earth-Science Reviews*, *209*, 103288. https://doi.org/10.1016/j.earscirev.2020.103288

Scandone, R. (1990). Chaotic collapse of calderas. *Journal of Volcanology and Geothermal Research*, *42*(3), 285–302. https://doi.org/10.1016/0377-0273(90)90005-Z

Scott, E. D., & Wilson, L. (2002). Plinian eruptions and passive collapse events as mechanisms of formation for Martian pit chain craters. *Journal of Geophysical Research*, *107*(4), 4–1. https://doi.org/10.1029/2000je001432

Sefton-Nash, E., Catling, D. C., Wood, S. E., Grindrod, P. M., & Teanby, N. A. (2012). Topographic, spectral and thermal inertia analysis of interior layered deposits in Iani Chaos, Mars. *Icarus*, *221*(1), 20–42. https://doi.org/10.1016/j.icarus.2012.06.036

Sharp, R. P. (1973). Mars: Fretted and chaotic terrains. *Journal of Geophysical Research*, *78*(20), 4073–4083. https://doi.org/10.1029/JB078i020p04073

Smith, D. E., Zuber, M. T., Jackson, G. B., Cavanaugh, J. F., Neumann, G. A., Riris, H., et al. (2010). The lunar orbiter laser altimeter investigation on the lunar reconnaissance orbiter mission. *Space Science Reviews*, *150*(1–4), 209–241. https://doi.org/10.1007/s11214-009-9512-y

Smith, D. E., Zuber, M. T., Solomon, S. C., Phillips, R. J., Head, J. W., Garvin, J. B., & Duxbury, T. C. (1999). The global topography of Mars and implications for surface evolution. *Science*, *284*(5419), 1495–1503. https://doi.org/10.1126/science.284.5419.1495

Spencer, J. R., & Fanale, F. P. (1990). New models for the origin of Valles Marineris closed depressions. *Journal of Geophysical Research*, *95*(B9), 14301–14313. https://doi.org/10.1029/JB095IB09P14301

Tanaka, K. L. (1997). Origin of valles marineris and noctis labyrinthus, mars, by structurally controlled collapse and erosion of crustal materials. In *28th Annual Lunar and Planetary Science Conference*, p. 413. Retrieved from https://ui.adsabs.harvard.edu/abs/1997LPI28.1413T/abstract

Tanaka, K. L. & Golombek, M. P. (1989). Martian tension fractures and the formation of grabens and collapse features at Valles Marineris. *Lunar and Planetary Science Conference, 19th, Houston, TX, Mar. 14-18, 1988, Proceedings (A89-36486 15-91)*, 383–396.Retrieved from http://articles.adsabs.harvard.edu/cgi-bin/nph-iarticle_query?bibcode=1989LPSC...19.383T&db_key=AST&page_ind=10&plate_select=NO&data_type=GIF&type=SCREEN_GIF&classic=YES

Thorey, C., Michaut, C., & Wieczorek, M. (2015). Gravitational signatures of lunar floor-fractured craters. *Earth and Planetary Science Letters*, *424*, 269–279. https://doi.org/10.1016/j.epsl.2015.04.021

Troll, V. R., Walter, T. R., & Schmincke, H.-U. (2002). Cyclic caldera collapse: Piston or piecemeal subsidence? Field and experimental evidence. *Geology Series*, *30*(2), 135–138. https://doi.org/10.1130/0091-7613(2002)030<0135:cccpop>2.0.co;2

Walter, T. R., & Troll, V. R. (2001). Formation of caldera periphery faults: An experimental study. *Bulletin of Volcanology*, *63*(2–3), 191–203. https://doi.org/10.1007/s004450100135

Walwer, D., Michaut, C., Pinel, V., & Adda-Bedia, M. (2021). Magma ascent and emplacement below floor fractured craters on the Moon from floor uplift and fracture length. *Physics of the Earth and Planetary Interiors*, *312*, 106658. https://doi.org/10.1016/j.pepi.2021.106658

Warner, N. H., Gupta, S., Kim, J.-R., Muller, J.-P., Le Corre, L., Morley, J., et al. (2011). Constraints on the origin and evolution of Iani Chaos, Mars. *Journal of Geophysical Research*, *116*(E6). E06003. https://doi.org/10.1029/2010JE003787

Weijermars, R., & Schmeling, H. (1986). Scaling of Newtonian and non-Newtonian fluid dynamics without inertia for quantitative modeling of rock flow due to gravity (including the concept of rheological similarity). *Physics of the Earth and Planetary Interiors*, *43*(4), 316–330. https://doi.org/10.1016/0031-9201(86)90021-X

Wieczorek, M. A., Neumann, G. A., Nimmo, F., Kiefer, W. S., Taylor, G. J., Melosh, H. J., et al. (2013). The crust of the moon as seen by GRAIL. *Science*, *339*(6120), 671–675. https://doi.org/10.1126/science.1231530

Wilson, L., & Head, J. W. (2018). Lunar floor-fractured craters: Modes of dike and sill emplacement and implications of gas production and intrusion cooling on surface morphology and structure. *Icarus*, *305*, 105–122. https://doi.org/10.1016/j.icarus.2017.12.030

Wilson, L., & Head, J. W., III (2002). Tharsis-radial graben systems as the surface manifestation of plume-related dike intrusion complexes: Models and implications. *Journal of Geophysical Research*, *107*(E8). https://doi.org/10.1029/2001je001593

Wyrick, D., Ferrill, D. A., Morris, A. P., Colton, S. L., & Sims, D. W. (2004). Distribution, morphology, and origins of Martian pit crater chains. *Journal of Geophysical Research*, *109*(E6). https://doi.org/10.1029/2004je002240

Zegers, T. E., Oosthoek, J. H. P., Rossi, A. P., Blom, J. K., & Schumacher, S. (2010). Melt and collapse of buried water ice: An alternative hypothesis for the formation of chaotic terrains on Mars. *Earth and Planetary Science Letters*, *297*(3–4), 496–504. https://doi.org/10.1016/j.epsl.2010.06.049